Materialwiss. Werkstofftech. **2020**, *51*, 706–712 **DOI** 10.1002/mawe.202000010

Synthesis and properties of bio-waste-based hydroxyapatite via hydrothermal process

Synthese und Eigenschaften von Hydroxylapatit auf Bioabfallbasis über einen hydrothermalen Prozess

C.K. Ng[1], Z.L. Ng[1], S. Ramesh[2, 3], C.Y. Tan[2], C.H. Ting[4], Y.D. Chuah[5], U. Sutharsini[6]

In this study, a facile hydrothermal method is applied to produce hydroxyapatite (HA) particles using egg shells as calcium precursors and fruit waste extracts (banana peel) as biomolecular templates at 150 °C for a reaction time period of 12 hours (h) and 24 hours. The sintering of the green samples of hydroxyapatite were conducted at 1250 °C in air for 2 h. The results showed that pectin extracted from banana peel extracts assisted in regulating crystal growth to obtain homogeneous hydroxyapatite powder, with higher purity observed for 24 h hydrothermal reaction time. Fourier-transform infrared spectroscopy (FTIR) spectra revealed the presences of phosphate (PO_4^{3-}) and hydroxyl (OH^-) groups in the powders. A relative density of 89.6 % was achieved for sintered hydroxyapatite compacts produced via hydrothermal method for 24 h. The sintered body was characterized by having high Vickers hardness of 5.35 GPa and good fracture toughness of 1.23 MPa$\sqrt{m}$, suitable for biomedical application.

Keywords: Hydroxyapatite **/** bio-waste **/** bio-ceramics **/** hydrothermal **/** mechanical properties

Schlüsselwörter: Hydroxylapatit **/** Bioabfall **/** Biokeramik **/** hydrothermal **/** mechanische Eigenschaften

[1] Tunku Abdul Rahman University College, Centre for Advanced Materials, Faculty of Engineering & Technology, Department of Materials Engineering, 53300, KUALA LUMPUR, MALAYSIA
[2] University of Malaya, Centre of Advanced Manufacturing & Materials Processing (AMMP), Faculty of Engineering, Department of Mechanical Engineering, 50603, KUALA LUMPUR, MALAYSIA
[3] Universiti Teknologi Brunei, Faculty of Engineering, Department of Mechanical Engineering, Tunku Highway,Mukim Gadong A, GADONG BE1410, NATION OF BRUNEI, THE ABODE OF PEACE
[4] Universiti Tunku Abdul Rahman, Lee Kong Chian Faculty of Engineering and Science, Department of Mechanical and Materials & Manufacturing Engineering, Jalan Sungai Long, Bandar Sungai Long, Cheras, 43000, KAJANG, MALAYSIA
[5] Universiti Tunku Abdul Rahman, Lee Kong Chian Faculty of Engineering and Science, Department of Mechatronics and BioMedical Engineering, Jalan Sungai Long, Bandar Sungai Long, Cheras, 43000, KAJANG, MALAYSIA
[6] University of Jaffna, Department of Physics, 40000, JAFFNA, DEMOCRATIC SOCIALIST REPUBLIC OF SRI LANKA

Corresponding author: C.K. Ng, Tunku Abdul Rahman University College, Centre for Advanced Materials, Faculty of Engineering & Technology, Department of Materials Engineering, 53300, KUALA LUMPUR, MALAYSIA,
E-Mail: ngck@tarc.edu.my

1 Introduction

Bone grafting is a surgical procedure that implants bone restorative materials into the bone defected site for its growth and healing. Most bone grafts are expected to be reabsorbed and replaced by the natural bone during the healing process. However, there are drawbacks associated with bone grafting, such as complications of bone resorption, infection, donor site morbidity, and strength reduction. This has stimulated extensive research interest in developing synthetic biomaterial substitutes using metal, polymer, and ceramic that emulate natural bone structure [1–2]. The ideal bone replacement is a biomaterial replacement resembling the biomechanical and biochemical properties of mineral bone and a porous structure to allow new cells to penetrate the structure and proliferate [3–4]. Conventional biocompatible metals such as titanium (Ti), tantalum (Ta), magnesium (Mg), and stainless steel are notable examples used as bone substitutes for its excellent fracture toughness and flexural strength. However, the main disadvantage of the non-biologic metallic substrates is their degradation upon interaction with body fluids, which could elicit the release of toxic metallic ions and cause inflammation [5]. The shortcoming of metallic implant biomaterials can be overcome by using hydroxyapatite as the implant biomaterial.

2 State of the art

Hydroxyapatite (HA), $Ca_{10}(PO_4)_6(OH)_2$, is the principle inorganic calcium phosphate mineral component that has been extensively used as an implant material for human bones and teeth for its remarkable properties that include biocompatibility, bioactivity, osteoconductivity, non-toxicity, and non-inflammatory nature [6]. Various techniques have been developed to produce bioactive hydroxyapatites to mimic natural bone characteristics. The synthesis techniques applied include the wet chemical precipitation, mechanochemical, sol-gel and hydrothermal [7–11]. Synthesized hydroxyapatites prepared from these production techniques often lack the presence of trace amounts of anionic and/or cationic in their lattice structure which are normally found in human bones. On the contrary, hydroxyapatite fabricated from natural resources and agricultural wastes such as egg shells, crab shells, and fish bones are non-stoichiometric due to the trace amount of ions incorporated in their lattice [12–15]. Egg shell consists mostly of calcium carbonate ($CaCO_3$) with trace number of bioinorganic ions such as sodium, strontium and magnesium that make it an attractive bio-waste derived calcium precursor for the synthesis of hydroxyapatites. These techniques involved the use of organic solvents or organic templating agents which are mostly harmful to the natural habitat and the ecosystem. Therefore, many recent studies have focused on synthesizing hydroxyapatite with the green materials, which are more environmentally friendly, sustainable and also lower in cost as compared to organic templates [16]. Consequently, the development of hydroxyapatite from natural biomaterials is of enormous significance in its application as bone-like implants.

3 Aim of the investigation

Egg shells comprise approximately 11 % of the total weight of the egg and are primarily consisting of calcium carbonate ($CaCO_3$). Pectin is an excellent biocompatible and biodegradable polysaccharide material with several noteworthy biological properties such as antimicrobial, anticoagulant, and anti-inflammatory. Pectin has shown promise in biomedical application for bone tissue regeneration [17]. Pectin based bio-composite is used to alter the degree of swelling in oral drug delivery. Pectin is also investigated as surface modifier for medical devices [18]. Pectin-based material is exploited to imitate the natural extracellular matrix to induce the proliferation of osteoblast. The ionic plant polysaccharides which are predominantly rich in carboxyl and hydroxyl groups, can improve the binding of calcium ions (Ca^{2+}) to form large number of nuclei for hydroxyapatite crystal growth [19]. The hybrid organic-inorganic material can offer favorable effect in bone fixation and repair of bone tissue defects.

The aim of the current study is to produce pectin mediated egg shell-based hydroxyapatite bio-ceramic with adequate strength, high purity, good physical properties, and biocompatibility via facile hydrothermal synthesis.

4 Materials and experimental details

Chicken egg shells were washed thoroughly and then crushed into powder in a pestle and mortar. About 2 g of the egg shell powder was dispersed in 20 cm^3 of 1 to 3 ratio of hydrochloric acid (HCL) and distilled water in accordance to Equation 1.

$$CaCO_3 + 2\ HCl \rightarrow CaCl_2 + H_2O + CO_2 \qquad (1)$$

20 g of cleaned banana peel was boiled in 250 cm^3 of water for 10 min and filtered. About 5 cm^3 of this banana peel filtrate was then poured into the egg shell solution and the mixture was stirred thoroughly. After that about 0.85 cm^3 (i. e. Ca/P molar ratio = 1.67) of 85 % phosphoric acid was added dropwise to the slowly stirred mixture. Ammonia solution (NH_4OH) was added to maintain the pH of the solution at 10. The expected reaction for this process is as follows:

$$10\ CaCl_2 + H_2O + 2\ NH_4OH + 6\ H_3PO_4 \rightarrow\ Ca_{10}(PO_4)_6(OH)_2 + 20\ HCl + 2\ NH_4 \qquad (2)$$

The hydroxyapatite slurry is poured into a polytetrafluoroethylene (Teflon)-lined stainless steel pressure vessel and hydrothermal synthesis took place at 150 °C for a reaction times of 12 h and 24 h (denoted as hydroxyapatite-12 and hydroxyapatite-24, respectively). The autoclave was allowed to cool to room temperature by natural cooling after hydrothermal treatment. The resulting hydroxyapatite precipitates were then filtered and washed with deionized water until all traces of chloride ions and ammonium ions were removed. The precipitates were then dried in an oven at 100 °C for 24 h. The hydroxyapatite dried cake was crushed in a pestle and mortar, and then sieved through 150 μm sieve to obtain a uniform sized hydroxyapatite powder. The hydroxyapatite powder was uniaxial compacted to form a circular disc. The hydroxyapatite disc samples were heated to 1250 °C at a ramp rate 10 °C/min in a conventional pressure less furnace with a dwell time of two hours.

The crystalline phases of the hydroxyapatite samples were analyzed using x-ray diffraction (XRD-6000, Shidmazu) with CuK_α radiation over the 2θ range of 20°–60°. The microstructural evolution of the hydroxyapatite samples was evaluated by scanning electron microscopy (SEM: SEC SNE-3000M Desktop Mini) equipped with energy dispersive x-ray (EDX). The characterization of the samples was conducted using Fourier transform infrared (FTIR: Spectrum 65, Perkin-Elmer). The bulk density of the sintered specimens were measured by using an electronic balance (Shimadzu AY220, Japan) in accordance to the Archimedes' principle with distilled water as the immersion medium. Relative density was calculated by taking the theoretical density of HA = 3.16 g/cm^3. The hardness of hydroxyapatite bio-ceramics was evaluated by the Vickers indentations method using a load of 0.2 Kgf. The cracks obtained from the Vickers indentation were used to determine the fracture toughness based on the relationship proposed below [20]:

$$K_{IC} = 0.016 \left(\frac{E \times 1000\ s^2}{H \times 9.8\ m}\right)^{1/2} \times \left(\frac{F}{c^{3/2}}\right) \qquad (3)$$

Where F is the applied load in Newton (N), c is the crack length measured from the center of the indent to the crack tip in meters (m), E is the Young's modulus in GPa, and H is the Vickers hardness in GPa. At low loads, Palmqvist cracks are favored, while at high loads fully developed median cracks result.

5 Results and discussion

5.1 X-ray diffraction

The x-ray diffraction plots of the hydroxyapatite powder synthesized via hydrothermal transformation with reaction times of 12 h and 24 h show that the as-synthesized hydroxyapatite powders have broadening diffraction peaks at 31.8°–32.8°, as compared to the hydroxyapatite samples sintered at 1250 °C for 2 h, *Figure 1*. This indicates that the hydroxyapatite powders have lower crystallization compared to the sintered compacts and this is in agreement with other reports for hydroxyapatite particles [21–22].

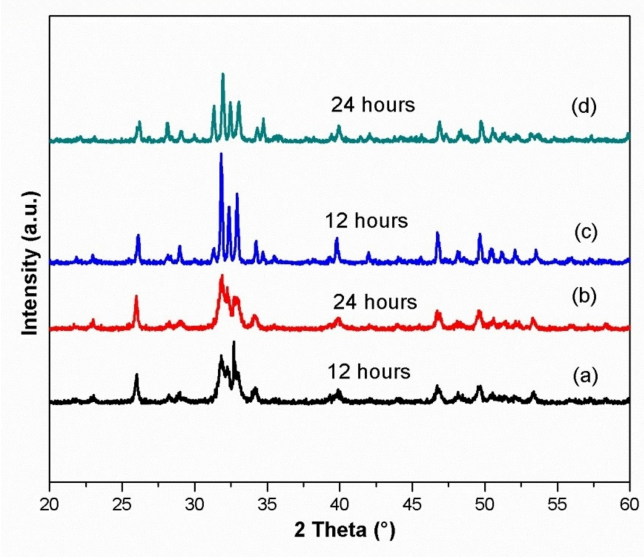

Figure 1. X-ray diffraction (XRD) plots of hydroxyapatite samples synthesized via hydrothermal method with reaction times of 12 h and 24 h. (a–b) powder, (c–d) samples sintered at 1250 °C.

5.2 Fourier transform infrared (FTIR) analysis

The first indication of the formation of hydroxyapatite is in the form of a strong complex broad Fourier-transform infrared spectroscopy band centered at about 1000 cm^{-1}–1100 cm^{-1} due to asymmetrical stretching mode of vibration for PO_4 group, *Figures 2–3*. From the broad Fourier-transform infrared spectroscopy spectrum of both synthesized hydroxyapatite powders, the asymmetric stretching (V3) modes of PO_4^{3-} ion are detected at around 1031 cm^{-1} and 1089 cm^{-1} for hydroxyapatite-12 powder and 1026 cm^{-1}, 1089 cm^{-1} for hydroxyapatite-24 powder. The symmetrical stretching modes (V1) of PO_4^{3-} ion are also found at around 962 cm^{-1} for hydroxyapatite-12 and hydroxyapatite-24 powders respectively. This indicates that both of the synthesized hydroxyapatite powders exhibited the characteristic bands of phosphate groups of the apatite structure. The stretching vibrations, ascribed to CO_3^{2-} at around 1464 cm^{-1} and 1457 cm^{-1} for hydroxyapatite-12 and hydroxyapatite-24 powders, respectively, are also present. The presence of CO_3^{2-} in the hydroxyapatite is associated with the egg shell which was used as the calcium source in the synthesis process. The intensities of CO_3^{2-} peak could be reduced by heat treatment at higher temperatures. Furthermore, the spectrum of hydroxyapatite has characteristic bands at 632 cm^{-1} and 3571 cm^{-1}, corresponding to OH-groups in the apatite lattice. The hydroxyl bands at 632 cm^{-1} and 3571 cm^{-1} are typical of highly crystalline hydroxyapatite sintered at high temperature. The liberation and stretching modes of the OH^- are

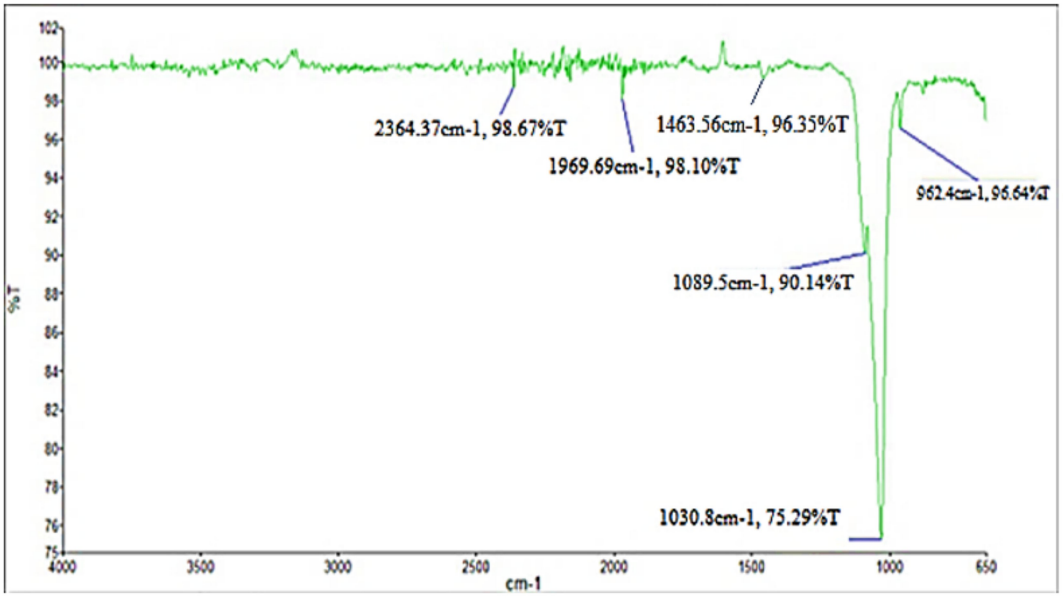

Figure 2. The Fourier-transform infrared spectroscopy spectrum of the hydroxyapatite powder synthesized via hydrothermal method with a reaction time of 12 h (hydroxyapatite-12).

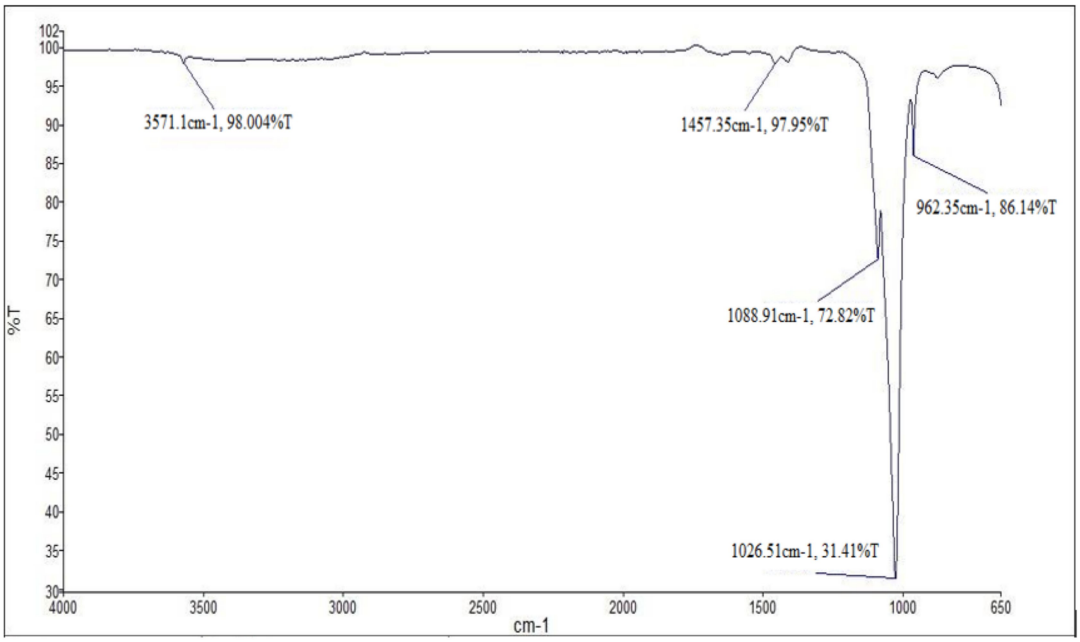

Figure 3. The Fourier-transform infrared spectroscopy spectrum of the hydroxyapatite powder synthesized via hydrothermal method with a reaction time of 24 h (hydroxyapatite-24).

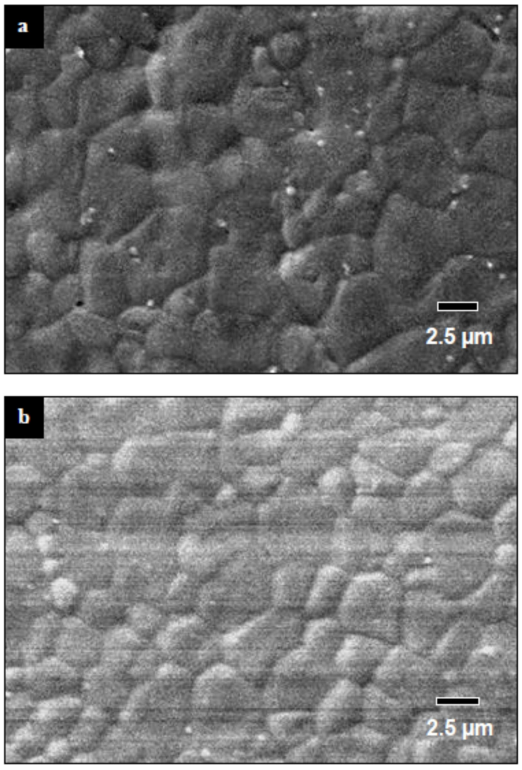

Figure 4. Scanning electron microscopy micrographs of sintered samples: (a) hydroxyapatite-12 and (b) hydroxyapatite-24.

detected at around 3571 cm^{-1} for hydroxyapatite-24 powder, which is a common features of hydroxyapatite.

5.3 Scanning electron microscope (SEM) and energy dispersive x-ray spectroscopy (EDS) analysis

The scanning electron microscopy micrographs of the sintered hydroxyapatite samples prepared via hydrothermal reaction at 150 °C for 12 h and 24 h are taken to measure the grain size, *Figure 4*.

Sintered hydroxyapatite-24 sample exhibited smaller average grain size (~4.07 µm) compared to sintered hydroxyapatite-12 sample (~4.83 µm). Hydroxyapatite samples with longer reaction time would promote the nucleation and growth of particles.

The bulk Ca/P molar ratios of hydrothermally synthesized hydroxyapatite were determined as 1.85 and 1.77, after 12 h and 24 h of hydrothermal reaction, respectively. The higher Ca/P ratio, above the stoichiometric value of 1.67 for hydroxyapatite, could be attributed to the presence of carbonate ions substituting the phosphate, thus indicating the presence of B-type carbonated hydroxyapatite. The substitution is believed to reduce the phosphorus

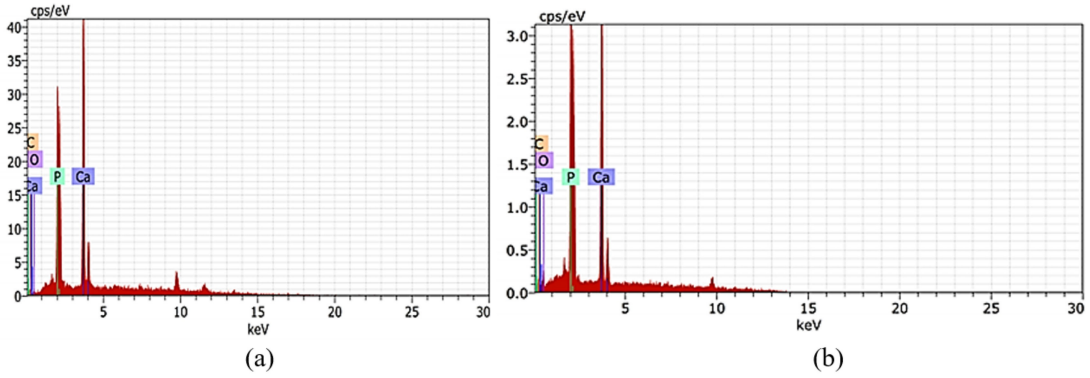

Figure 5. The energy dispersive x-ray spectrum and elemental composition of sintered samples: (a) hydroxyapatite-12 and (b) hydroxyapatite-24.

content of hydroxyapatite, thus resulting in a higher value of the Ca/P ratio. The energy dispersive x-ray analysis indicates the presence of calcium (Ca), phosphorus (P), and oxygen (O) which are elements present in the hydroxyapatite phase, *Figure 5*.

5.4 Mechanical properties

The relative densities of 87.3 % and 89.6 % were obtained for sintered hydroxyapatite-12 and hydroxyapatite-24 samples, respectively. As biosynthetic bone implants, the formations of pores are advantageous since they permit tissue growth on the implants and allows body fluid circulation. The sintered hydroxyapatite-24 sample revealed a higher Vicker hardness of 5.35 GPa and fracture toughness of 1.23 MPa$\sqrt{}$m, as compared to sintered hydroxyapatite-12 sample which had a Vickers hardness of 4.76 GPa and fracture toughness of 1.08 MPa$\sqrt{}$m. The major factor influencing the fracture toughness is the grain size of the sintered body. Fine-grained matrix is favorable as it leads to more grain boundaries per unit volume which can impede the movement of dislocations. When the dislocations are effectively inhibited, the permanent deformation of the sample can be prevented and hence giving the sintered sample of finer grain size a higher fracture resistance.

6 Conclusions

The current study presents a hydrothermal method to produce pure and stable hydroxyapatite powder using egg shells and banana peel extracts as the starting precursors. Hydroxyapatite powder was synthesized via hydrothermal technique with 12 h and 24 h of reaction times at 150 °C. The Ca/P ratio for the hydroxyapatite-12 and hydroxyapatite-24 sintered samples were greater than the stoichiometric value of hydroxyapatite (1.67). A high Ca/P ratio could be attributed to the presence of carbonate ions substituting the phosphate, thus promoting the presence of a B-type carbonated hydroxyapatite. The sintered hydroxyapatite compacts derived from egg shells exhibited better mechanical properties (i. e. Vickers hardness of 5.35 GPa and fracture toughness of 1.23 MPa$\sqrt{}$m) if compared to typical calcium phosphate ceramics for biomedical applications. This research has demonstrated the viability of egg shell-derived hydroxyapatite to be used as a potential biomaterial for bone substitutions.

Acknowledgements

This research was supported under the FRGS grant No. FP020-2018 A.

7 References

[1] S. Titsinides, G. Agrogiannis, T. Karatzas, *Japanese Dent. Sci. Rev.* **2019**, *55*, 26.

[2] W. Wang, K.W. Yeung, *Bioactive Mater.* **2017**, *2*, 224.

[3] P. Baldwin, D.J. Li, D.A. Auston, H.S. Mir, R.S. Yoon, K.J. Koval, *J. Orthopaedic Trauma* **2019**, *33*, 203.

[4] A. Niakan, S. Ramesh, P. Ganesan, C.Y. Tan, J. Purbolaksono, H. Chandran, W.D. Teng, *Ceram. Int.* **2015**, *41*, 3024.

[5] K. Alvarez, H. Nakajima, *Mater.* **2009**, *2*, 790.

[6] D.S. Gomes, A.M.C. Santos, G.A. Neves, R. R. Menezes, *Cerâmica* **2019**, *65*, 282.

[7] N. Monmaturapoj, *J Met. Mater. and Minerals* **2008**, *18*, 15.

[8] K.C.B. Yeong, J. Wang, S.C. Ng, *Biomaterials* **2001**, *22*, 2705.

[9] F. Bakan, O. Laçin, H. Sarac, *Powder Technol.* **2013**, *233*, 295.

[10] M.P. Ferraz, F.J. Monteiro, C.M. Manuel, *J. App Biomaterials and Biomechanics* **2004**, *2*, 74.

[11] V. Jokanović, D. Izvonar, M.D. Dramićanin, B. Jokanović, V. Živojinović, D. Marković, B. Dačić, *J. Mater. Sci: Mater. in Med.* **2006**, *17*, 539.

[12] P. Kamalanathan, S. Ramesh, L.T. Bang, A. Niakan, C.Y. Tan, J. Purbolaksono, H. Chandran, W.D. Teng, *Ceram. Int.* **2014**, *40*, 16349.

[13] S. Ramesh, A.N. Natasha, C.Y. Tan, L.T. Bang, C.Y. Ching, H. Chandran, *Ceram. Int.* **2016**, *42*, 7824.

[14] S. Endang, N. Rauf, *In J. Phys.: Conf. Series. IOP Publishing* **2019**, *1242*, 012032.

[15] M. Boutinguiza, J. Pou, R. Comesaña, F. Lusquiños, A. De Carlos, B. León, *Mater. Sci. Eng. C.* **2012**, *32*, 478.

[16] D. Gopi, K. Kanimozhi, N. Bhuvaneshwari, J. Indira, L. Kavitha, *Spectrochim Acta A: Molecular and Biomolecular Spectroscopy* **2014**, *118*, 589.

[17] P. Coimbra, P. Ferreira, H.C. de Sousa, P. Batista, M.A. Rodrigues, I.J. Correia, M.H. Gil, *Int. J. Biological Macromolecules* **2011**, *48*, 112.

[18] M. Morra, C. Cassinelli, G. Cascardo, M.D. Nagel, C. Della Volpe, S. Siboni, D. Maniglio, M. Brugnara, G. Ceccone, H.A. Schols, P. Ulvskov, *Biomacromolecules* **2004**, *5*, 2094.

[19] W. Fang, H. Zhang, J. Yin, B. Yang, Y. Zhang, J. Li, F. Yao, *Crystal Growth & Design* **2016**, *16*, 1247; Design **2016**, 16, 1247.

[20] G.R. Anstis, P. Chantikul, B.R. Lawn, D.B. Marshall, *J. Am. Ceram. Soc.* **1981**, *64*, 533.

[21] M.L. Martins, I.L. Iessi, M.P. Quintino, D.C. Damasceno, C.G. Rodrigues, *Mater. Chem. and Phys.* **2019**, *240*, 122166.

[22] S.A. Ibraheem, E.A. Audu, J.A. Adudu, J.T. Barminas, V. Ochigbo, A. Igunnu, S.O. Malomo, *Surf. and Interfaces* **2019**, *17*, 100360.

Received in final form: February 7th 2020

